Pharmaceutical Sciences and Drug Design
ISSN: 3062-4428
2024, Volume 4, Page No: 182-196

Available online at: www.galaxypub.co/page/journals

Galaxy Publication

Enhanced Therapeutic Efficacy of Dexamethasone in Experimental Ulcerative Colitis via Mucoadhesive Nanoparticle-Based Enema Delivery

Caroline Fischer[1]*, Lukas Graf[1]

[1]Department of Biotechnology, Faculty of Engineering, ETH Zurich, Zurich, Switzerland.

***E-mail** ✉ caroline.fischer.ch@outlook.com

Received: 11 September 2024; **Revised:** 04 December 2024; **Accepted:** 07 December 2024

ABSTRACT

Glucocorticoids (GCs) are the primary treatment for ulcerative colitis (UC), but their long-term use is associated with severe systemic toxicity and side effects. Local delivery via enema can enhance GC concentrations at the site of inflammation in the distal colon while minimizing systemic exposure. However, frequent diarrhea in UC patients often shortens colonic residence time, limiting the therapeutic efficacy of GCs.This study aimed to develop mucoadhesive nanoparticles (NPs) carrying different dexamethasone derivatives (DDs) that can adhere to the positively charged inflamed colonic mucosa through electrostatic interactions after enema administration, thereby increasing local drug concentration and achieving targeted therapy for UCTwo dexamethasone derivatives, dexamethasone hemisuccinate and dexamethasone phosphate, were synthesized. Core PEI-DDs NPs were prepared via electrostatic interaction between the cationic polymer polyethyleneimine (PEI) and DDs. Subsequently, the natural polyanionic polysaccharide sodium alginate (SA) was coated onto the NP surface to form SA-PEI-DDs NPs. The formulations were characterized for in vitro stability, drug release, and colonic mucosal adhesion both in vitro and in vivo. Therapeutic efficacy was evaluated in TNBS-induced colitis mice by monitoring body weight, disease activity index (DAI), myeloperoxidase (MPO) activity, pro-inflammatory cytokine levels, and histopathological changes via hematoxylin and eosin staining.The structures of the DDs were confirmed by 1H-NMR and MS. The NPs exhibited negative surface charges, high drug loading efficiency, and particle sizes that differed significantly between formulations. They showed good stability and sustained drug release under simulated colonic conditions. The negative surface charge promoted adhesion to positively charged inflamed mucosa, enhancing local retention of the NPs at the colitis site. In vivo, SA-PEI-DDs NPs demonstrated superior therapeutic effects compared to free dexamethasone in TNBS-induced colitis mice.Mucoadhesive SA-PEI-DDs nanoparticles represent a promising nano-enema strategy for UC, enabling enhanced colonic targeting, prolonged drug retention, and improved therapeutic outcomes.

Keywords: Ulcerative colitis, Glucocorticoids, Mucoadhesive nanoparticles, Polyethyleneimine, Sodium alginate

How to Cite This Article: Fischer C, Graf L. Enhanced Therapeutic Efficacy of Dexamethasone in Experimental Ulcerative Colitis via Mucoadhesive Nanoparticle-Based Enema Delivery. Pharm Sci Drug Des. 2024;4:182-96. https://doi.org/10.51847/4cQCAkalAM

Introduction

Ulcerative colitis (UC) is a chronic inflammatory bowel disease marked by diffuse mucosal inflammation, primarily affecting the distal colon and rectum [1, 2]. Its long-term, relapsing nature significantly impairs patients' quality of life. Glucocorticoids (GCs) are the first-line therapy for moderate-to-severe UC due to their ability to suppress inflammatory mediators (e.g., leukotrienes, prostaglandins), cytokines (e.g., interleukins, TNF-α, interferon), and nitric oxide (NO) via transcriptional regulation [3–6]. However, systemic side effects—including endocrine, cardiovascular, skeletal, ophthalmic, neurological, and gastrointestinal disorders—arise from prolonged oral GC administration [7, 8]. Targeted delivery of GCs directly to the inflamed colonic tissue can enhance local anti-inflammatory effects while reducing systemic toxicity.

Enema administration is widely employed for localized treatment of intestinal disorders [9–11]. Approximately two-thirds of UC patients present with inflammation in the distal colon, which is ideally addressed via local enema

delivery [12, 13]. This route allows direct drug deposition at the site of inflammation, improving local tissue drug levels while avoiding high systemic exposure [14, 15]. However, frequent diarrhea in UC patients reduces colonic drug residence time, limiting therapeutic efficacy [16, 17]. Nano drug delivery systems (NDDSs) can address this challenge. In UC, epithelial barrier dysfunction increases mucosal permeability, enabling NDDSs to preferentially accumulate in inflamed tissue via an epithelial-enhanced permeability and retention (eEPR) effect [18, 19]. Additionally, inflamed colonic tissues exhibit depleted mucus and accumulation of positively charged proteins, such as antimicrobial peptides and bactericidal/permeability-increasing proteins, creating a highly positive microenvironment [20–22]. NDDSs with negative surface charges can electrostatically adhere to these inflamed sites, reducing drug loss due to diarrhea and enhancing site-specific delivery.

Effective enema therapy requires high local GC concentrations, which depend on carriers with efficient drug-loading capabilities [23]. However, most NDDSs struggle to achieve high GC loading due to the hydrophobic nature of GCs [24]. Converting GCs into water-soluble derivatives combined with oppositely charged polymers enables efficient nanoparticle formation and high drug loading [25]. In this study, dexamethasone (Dex) was selected as a model GC, and two anionic derivatives were synthesized via esterification. These derivatives were self-assembled with the cationic polymer polyethyleneimine (PEI) to form positively charged PEI-DDs nanoparticles (NPs). PEI, a cation-rich polymer commonly used for nucleic acid and protein delivery, also exhibits immunomodulatory effects by binding negatively charged lipopolysaccharides (LPS) and inhibiting TNF-α expression in macrophages, thereby attenuating inflammation [26–30]. The multiple amino groups in PEI facilitate electrostatic, hydrogen bonding, and hydrophobic interactions with DDs, enabling efficient nanoparticle formation and drug encapsulation.

Sodium alginate (SA), a natural polysaccharide derived from kelp or sargassum, is widely used in biomedical applications due to its low toxicity, biocompatibility, and biodegradability [31, 32]. Its mucoadhesive properties allow interaction with mucin and enhance mucus viscosity, promoting retention at mucosal surfaces [33]. In this study, SA was coated onto PEI-DDs NPs to form bilayer SA-PEI-DDs NPs (Scheme 1), designed for enema administration. The electrostatic interaction between negatively charged SA and positively charged inflamed mucosa enhances nanoparticle adhesion, increases local drug concentration, improves therapeutic outcomes, and reduces systemic toxicity. This strategy offers a novel approach for targeted GC therapy in UC.

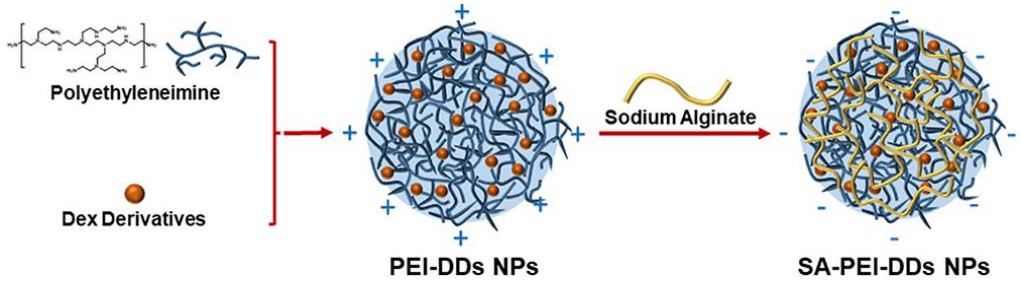

Scheme 1. Schematic illustration of the preparation of SA-PEI-DDs nanoparticles.

Materials and Methods

Dexamethasone (Dex), 2,4,6-trinitrobenzenesulfonic acid (TNBS), and fluorescein isothiocyanate (FITC) were sourced from Sigma-Aldrich Co. (St. Louis, MO, USA). Succinic anhydride, 4-dimethylaminopyridine (4-DMAP), pyrophosphoryl chloride, triethylamine, O-Dianisidine dihydrochloride (ODD), and EDTA were obtained from Aladdin Chemistry Co. Ltd. (Shanghai, China). Dimethyl sulfoxide (DMSO), ethanol, ethyl acetate, pyridine, polyethyleneimine (PEI), sodium alginate, calcium chloride, potassium dihydrogen phosphate, and sodium hydroxide were purchased from Kermel Chemical Co. Ltd. (Tianjin, China). All other reagents were of analytical grade and used as received.

Animal studies

Male BALB/c mice weighing 20 ± 2 g were acquired from the Laboratory Animal Center of Xi'an Jiaotong University. Mice were housed under controlled temperature (20–25 °C) and humidity (50–60%), with free access to food and water. Animals were acclimated for one week prior to experiments. All procedures followed

institutional ethical guidelines and were approved by the Institutional Animal Care and Use Committee of Xi'an Jiaotong University (Approval No. XJTULAC 2019–068).

Synthesis of Dexamethasone Derivatives (DDs)

1. *Dexamethasone Hemisuccinate (DSH):* Dexamethasone (1 g, 2.55 mmol) was dissolved in anhydrous acetone with 4-DMAP. Succinic anhydride (0.51 g, 5.10 mmol) was added, followed by dropwise triethylamine. The reaction was allowed to proceed at room temperature for 1 h. Insoluble impurities were removed by filtration, and the solvent was evaporated under reduced pressure. The crude residue was dissolved in absolute ethanol, mixed with distilled water at 60 °C to precipitate DSH, and recrystallized by redissolution in acetone and cooling at 4 °C for 24 h. The product was washed with 25% ethanol and dried to obtain white crystalline DSH.
2. *Dexamethasone Phosphate (DSP):* Dexamethasone (1 g, 2.55 mmol) was dissolved in anhydrous tetrahydrofuran, and pyrophosphoryl chloride was slowly added while maintaining a low temperature. The mixture reacted for 1 h, followed by addition of deionized water and heating to 60 °C. Na2CO3 was added for 30 min to complete the reaction. The resulting product was filtered, precipitated by dropwise addition of hydrochloric acid, washed repeatedly, and dried to yield white DSP powder.

Both DSH and DSP were characterized by ^1H-NMR (Bruker, Germany) and high-resolution mass spectrometry (HRMS, Thermo Scientific Q Exactive, USA).

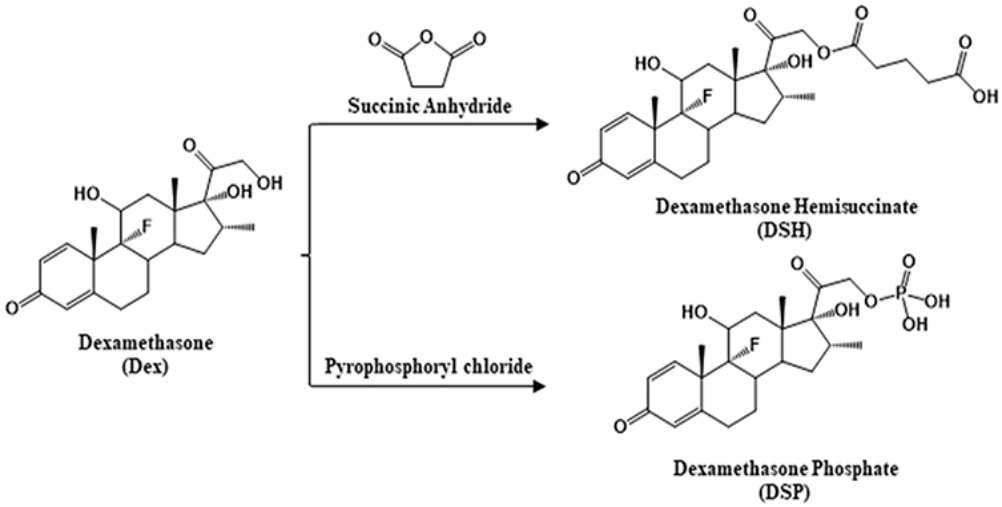

Figure 1. Synthetic schematic diagram of DSH and DSP

The in vitro analytical methods for DDs were established by first dissolving 10 mg of either DSH or DSP in 10 mL volumetric flasks with methanol to prepare a 1 mg/mL stock solution. The maximum absorption wavelength for each derivative was determined by further diluting the stock solutions to 0.01 mg/mL and scanning using a UV-visible spectrophotometer (UV-2550, Shimadzu, Japan) over the 200–800 nm range, which was subsequently used as the detection wavelength for all analyses [34]. Standard calibration curves were constructed by preparing methanol solutions of the glucocorticoid derivatives at 0.1 mg/mL and diluting aliquots of 0.5, 1, 1.5, 2, and 2.5 mL to 10 mL with methanol, resulting in final concentrations of 0.005, 0.01, 0.015, 0.02, and 0.025 mg/mL. Absorbance values were measured against a blank methanol solution, and standard curves were generated by plotting absorbance versus concentration. Precision was evaluated by measuring samples of three concentrations (0.005, 0.015, and 0.025 mg/mL) five times within a day for intra-day and across five days for inter-day assessments, with relative standard deviation (RSD) calculated. Recovery tests were performed by spiking these samples with DDs equivalent to 80%, 100%, and 120% of the initial content, and the percentage recovery was determined [34].

For the preparation of SA-PEI-DDs nanoparticles (NPs), 10 mg of DDs was mixed with 10 mg of PEI and dissolved in dimethyl sulfoxide (DMSO). This solution was placed in a dialysis bag (MWCO 3.5 kDa) and dialyzed against deionized water to allow the negatively charged DDs and cationic PEI to self-assemble via electrostatic interactions into PEI-DDs NPs. The dialysate was refreshed every 6 hours, and after 24 hours, the

nanoparticles were collected and freeze-dried. For surface modification, a suspension of PEI-DDs NPs in deionized water was prepared, and sodium alginate (SA) solution was added dropwise under stirring for 30 minutes at room temperature. The resulting SA-PEI-DDs NPs were purified through repeated washing, centrifugation, and lyophilization. The particle size, zeta potential, and polydispersity index (PDI) were measured using dynamic light scattering (DLS, Malvern Zetasizer Nano ZS, UK), and the morphology was examined using transmission electron microscopy (TEM, H600, Hitachi, Japan). During the fabrication process, factors including DDs concentration, pH, PEI molecular weight, SA concentration, and SA-to-PEI ratio significantly influenced nanoparticle formation, and single-factor experiments were conducted to systematically evaluate these effects.

Furthermore, the drug-loading coefficient (DL%) and entrapment efficiency (EE%) of DDs were calculated by the following equations, respectively:

$$DL\% = W_t/W_s 100\% \quad (1)$$

$$EE\% = W_1/W_0 100\% \quad (2)$$

Where W_t represented the weights of DDs in the final nanoparticles; W_s represented the weights of all components in the final nanoparticles. W_0 represented the weights of the feeding DDs.

The stability and in vitro release behavior of SA-PEI-DDs nanoparticles (NPs) were evaluated using dynamic light scattering (DLS). SA-PEI-DDs NPs (5 mL) were incubated in media simulating different gastrointestinal environments, including artificial gastric juice (pH 1.2), artificial small intestinal juice (pH 6.8), and artificial colon juice (pH 7.4), for 0, 0.5, 2, 4, 8, and 12 hours. At each predetermined time point, 1 mL of the solution was withdrawn, and particle size changes were measured to assess NP stability [35].

The in vitro release of DDs from SA-PEI-DDs NPs was investigated using two experimental setups to mimic oral and enema administration. For oral simulation, 5 mL of NPs solution was sequentially incubated in artificial gastric juice for 2 hours, small intestinal juice for 4 hours, and colon juice for 6 hours. For enema simulation, NPs solution was incubated only in colon juice (pH 7.4) for 12 hours. At predetermined intervals, 1 mL samples were collected and replaced with fresh medium. DDs concentrations in the samples were measured according to the previously established analytical methods, and cumulative release rates were calculated. All experiments were performed in triplicate, and results were expressed as the ratio of the measured value to the initial concentration [35].

The adhesion of SA-PEI-DDs NPs to isolated colonic mucosa was assessed using normal and inflamed mouse colonic tissues. Suspensions of PEI-DDs NPs and SA-PEI-DDs NPs were prepared, and their particle count rates (Kcps) were measured by DLS. Experimental colitis was induced in mice by intracolonic administration of 2,4,6-trinitrobenzenesulfonic acid (TNBS) dissolved in 50% ethanol, and colons were harvested after 12 hours, washed, and cut into 3 cm longitudinal segments. Tissue samples were incubated with 0.5 mL of NP suspensions at 37 °C for 2 hours in the dark, after which the decrease in Kcps was measured to quantify NP adhesion. Normal saline-treated mice were used as healthy controls [35].

In vivo adhesion studies employed fluorescein isothiocyanate (FITC) as a model to prepare SA-PEI-FITC NPs. Experimental colitis was induced as described, and FITC solution, PEI-FITC NPs, or SA-PEI-FITC NPs (1 mL) were administered via enema. After 2 hours, mice were sacrificed, colons were excised, longitudinally dissected, and washed, then observed under a confocal laser scanning microscope (CLSM, Leica TCS SP8, Germany) to evaluate fluorescence intensity. Healthy mice receiving saline instead of TNBS were used as controls [35].

The therapeutic efficacy of SA-PEI-DDs NPs was tested in TNBS-induced colitis mice. Mice were divided into six groups: (1) control (no colitis, enema saline, n=10), (2) TNBS (n=10), (3) TNBS+Dex (enema 70 μg/kg Dex, n=10), (4) TNBS+SA-PEI-DSH NPs (enema 70 μg/kg DSH, n=10), and (5) TNBS+SA-PEI-DSP NPs (enema 70 μg/kg DSP, n=10). Treatments were initiated 12 hours after colitis induction. Body weight changes, fecal characteristics, and fecal occult blood were recorded daily to calculate the disease activity index (DAI). The experiment lasted 5 days, after which survival rates were determined. Distal colons were collected, washed with ice-cold saline, and divided for myeloperoxidase (MPO) activity assays and histopathological analysis. For MPO measurement, tissue samples were homogenized in ten volumes of phosphate buffer (50 mM K2HPO4, pH 6.0) containing 0.5% HTAB, centrifuged, and the precipitate re-homogenized with phosphate buffer containing HTAB and 10 mM EDTA. MPO activity was determined based on the hydrogen-peroxide-dependent oxidation of o-dianisidine dihydrochloride (ODD), expressed as U/g tissue. Pro-inflammatory cytokines TNF-α, IL-6, and IL-1β

were quantified from colon homogenates using ELISA kits (Beyotime Biotechnology, Shanghai, China) following the manufacturer's instructions [35].

Table 1. The assay criteria of o-benzidine to determine the fecal occult blood of mice

Results	Phenomenon
Normal	No color occurred after adding reagents for 2 min
Occult blood	Green or light green appears after adding reagent for 2min
Occult blood+	Blue-green or dark green appears after adding reagent for 10s
Occult blood++	Blue or blue-green appears after adding reagent for 5–20s
Occult blood+++	Dark blue appears immediately after the reagent is added

Table 2. Disease activity index scoring criteria

Weight Loss	Character of Faeces	Occult Blood	Score
<0%	Normal	Normal	0
1–5%	Loose	Occult blood+	1
5–10%		Occult blood++	2
10–15%	Diarrhea	Occult blood+++	3
>15%		Visible blood in the stool	4

Statistical analysis

In this study, all quantitative results were presented as mean ± SD. Results in stability and in vitro release behavior study, mucoadhesion study, and anti-experimental ulcerative colitis study were analyzed by one-way ANOVA and LSD test using SPSS Statistical Software (v.22; IBM, Chicago, IL, USA). $p < 0.05$ was considered to be statistically significant.

Results and Discussion

Characterization and in vitro analytical method development for dexamethasone derivatives

Glucocorticoids (GCs) are potent anti-inflammatory agents that treat ulcerative colitis (UC) through several mechanisms, including decreasing capillary permeability to reduce edema and exudation, modulating glucocorticoid receptor activity to suppress NF-κB–mediated pro-inflammatory factor production, inhibiting cyclooxygenase and promoting lipocortin synthesis to reduce prostaglandin and leukotriene formation, regulating inflammatory gene expression to limit cytokine release, and reducing neutrophil and macrophage accumulation at sites of inflammation [1–6]. Despite their therapeutic benefits, long-term oral GC administration is associated with severe systemic side effects, highlighting the need for targeted delivery to inflamed colonic tissue to enhance local efficacy while limiting systemic exposure [7, 8]. Previous studies have shown that localized enema delivery of low-dose GCs can improve therapeutic outcomes in UC patients [9–11].

In this work, two dexamethasone derivatives (DDs), dexamethasone hemisuccinate (DSH) with a carboxylate group and dexamethasone phosphate (DSP) with a phosphate group, were synthesized through esterification. These derivatives were designed to form a nano-drug delivery system capable of adhering to inflamed colonic mucosa, thereby increasing the local retention and concentration of dexamethasone and improving its therapeutic effect.

DSH was prepared by reacting dexamethasone with succinic anhydride, whereas DSP was obtained using pyrophosphoryl chloride. The chemical structures of the derivatives were verified by ^1H-NMR and high-resolution mass spectrometry (MS). In the case of DSH, ^1H-NMR (600 MHz, DMSO-d6, δ ppm) displayed characteristic peaks at 0.886 (d, 3H, C16-H), 1.030 (s, 3H, C18-H), 1.614 (s, 3H, C19-H), 2.744 (m, 4H, C22-H, C23-H), 6.103 (s, 1H, C4-H), 6.034 (d, 1H, C2-H), and 7.427 (d, 1H, C1-H), with an MS [M+H]+ peak at 493.2. For DSP, ^1H-NMR (600 MHz, DMSO-d6, δ ppm) showed signals at 0.762 (m, 3H, C18-H), 1.365 (d, 3H, C22-H), 2.200 (m, 3H, C19-H3), 2.502 (s, 1H, C16-H), 5.108 (s, 1H, C4-H), 5.407 (m, 1H, C2-H), and 5.562 (m, 1H, C1-H), while the MS protonated molecular ion appeared at 463.2. These analyses confirmed the successful synthesis of both dexamethasone derivatives, which were subsequently used to develop the mucoadhesive nanoparticle delivery system.

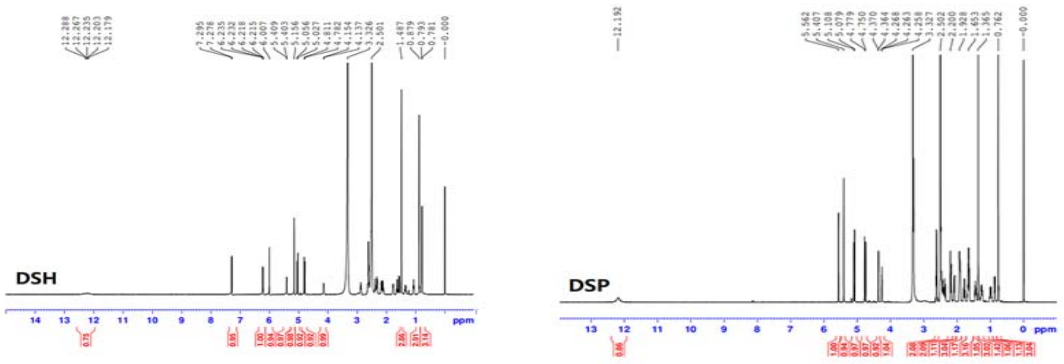

a) b)

Figure 2. ^{1}H-NMR spectrum of DSH (**a**) and DSP (**b**)

In the development of in vitro analytical methods for dexamethasone derivatives (DDs), their maximum absorbance wavelength was determined to be 241 nm using UV-visible spectroscopy. Within the concentration range of 0.005–0.025 mg/mL, the peak areas of the DDs displayed a strong linear correlation with the theoretical concentrations. Precision tests showed that the intra-day and inter-day relative standard deviations (RSDs) for the derivatives were below 15% across three concentrations. Recovery experiments indicated that the added sample recovery ranged from 99.64% to 100.71%, with no significant differences among the concentrations tested. Collectively, these findings demonstrate that the method provided acceptable reproducibility and recovery across the studied concentration range.

For the preparation and characterization of SA-PEI-DDs nanoparticles (NPs), the mucoadhesive systems were generated via the spontaneous self-assembly of hydrophilic or amphiphilic polymers, driven by multiple noncovalent interactions including electrostatic forces, hydrogen bonding, van der Waals forces, hydrophobic interactions, and π-π stacking. These interactions confer structural stability and favorable thermodynamic properties to the nanoparticles [36–38]. Initially, hydrophobic dexamethasone was chemically modified with acidic anhydrides and acid chlorides to produce water-soluble, negatively charged DDs. These derivatives were then complexed with the cationic polymer polyethyleneimine (PEI) via electrostatic interactions to form PEI-DDs NPs. Subsequently, the nanoparticles were coated with the naturally occurring polyanionic polysaccharide sodium alginate (SA), yielding SA-PEI-DDs NPs with surface charge inversion.

Several factors were found to significantly influence the particle size, zeta potential, and dispersibility of the SA-PEI-DDs NPs. As shown in **Figures 3a and 3b**, increasing DDs concentration led to a continuous reduction in particle size, zeta potential, and polydispersity index (PDI). This effect can be attributed to the higher negative charge density at elevated DDs concentrations, which enhanced electrostatic interactions with PEI. Furthermore, hydrophobic interactions and hydrogen bonding associated with dexamethasone's hydroxyl groups further strengthened the assembly, limiting PEI aggregation and promoting formation of smaller, more stable nanostructures. The influence of solution pH is illustrated in **Figures 3c and 3d**, where the smallest particle sizes were observed at neutral pH (pH 7). Both acidic and alkaline conditions increased particle size, likely due to disruption of electrostatic coupling by H^+ and OH^- ions, which also affected zeta potential and dispersibility. Notably, PEI-DSP NPs exhibited smaller particle sizes compared with PEI-DSH NPs, reflecting the stronger electrostatic interactions between the more negatively charged phosphate group of DSP and PEI, resulting in denser nanostructures.

The molecular weight of PEI also played a critical role in nanoparticle formation. Low molecular weight PEI (Mn = 1800) formed NPs with larger particle sizes due to fewer amino groups, which weakened electrostatic interactions with DDs. In contrast, high molecular weight PEI (Mn = 25,000) provided a greater number of amino groups, facilitating stronger interactions with DDs and yielding structurally robust nanoparticles.

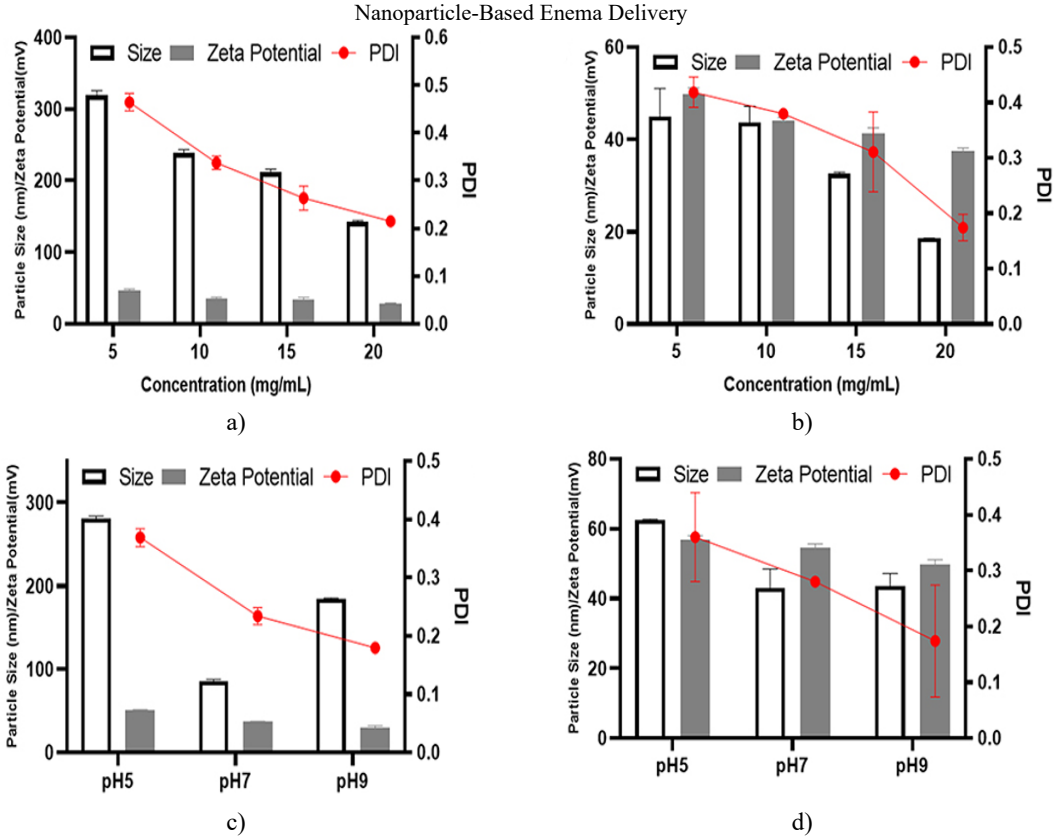

Figure 3. Illustrates the effects of Dex derivative (DDs) concentration and pH on the formation of PEI-DDs nanoparticles (NPs). Panels A and B show the influence of varying DSH and DSP concentrations on the particle size, zeta potential, and polydispersity index (PDI) of PEI-DSH and PEI-DSP NPs, respectively. Panels c and d depict how different pH values affect these parameters for PEI-DSH NPs (c) and PEI-DSP NPs (d) (mean ± SD, n = 3).

Sodium alginate (SA) is a critical component in constructing the final nanoparticles, as its concentration plays a central role in achieving surface charge inversion and promoting adhesion to inflammatory colonic mucosa. Additionally, the mass ratio of SA to PEI impacts the morphology, surface potential, and dispersibility of the resulting SA-PEI-DDs NPs. This effect is likely due to enhanced electrostatic interactions between the high-molecular-weight anionic polysaccharide SA and cationic PEI. Notably, precipitation occurred at an SA concentration of 2 mg/mL and a SA:PEI ratio of 0.5:1, likely because excessive SA rapidly aggregated with PEI through electrostatic adsorption. PEI-DDs NPs prepared with DSH exhibited larger particle sizes, which further increased upon SA coating, ultimately leading to precipitation.

These findings indicate that SA adsorbs onto the surface of PEI-DDs NPs via electrostatic interactions, causing an increase in particle size and reversing the surface charge to produce negatively charged SA-PEI-DDs NPs. Based on these observations, the optimized formulation of SA-PEI-DDs NPs was determined as follows: PEI molecular weight of 25,000, pH 7, Dex derivative and SA concentrations of 20 mg/mL and 1 mg/mL, respectively, and an SA:PEI feed ratio of 1:1. Characterization of the final nanoparticles prepared under these conditions is summarized in **Table 3**, and their morphology was confirmed by TEM **(Figure 4)**. The results demonstrated that SA coating significantly increased particle size. Due to stronger electrostatic interactions between DSP and PEI compared with DSH, PEI-DSP and SA-PEI-DSP NPs were smaller than their DSH counterparts. The final SA-PEI-DDs NPs exhibited strong negative surface charge and achieved high drug-loading efficiency (drug-loading coefficients >15%), enhancing their adhesion to positively charged colonic inflammatory mucosa and improving therapeutic efficacy by increasing local Dex absorption at the site of inflammation.

Table 3. Characterization data of SA-PEI-GC NPs (Mean ± SD, n = 3)

Parameters	SA-PEI-DSH-NPs	SA-PEI-DSP-NPs
Particle Size (nm)	196.33 ± 0.75	94.36 ± 2.28

Zeta Potential (mV)	−34.63 ± 0.77	−46.19 ± 0.25
PDI	0.25 ± 0.020	0.27 ± 0.010
Drug-loading coefficient (%)	27.40 ± 0.080	19.060 ± 0.26
Entrapment efficiency (%)	54.80 ± 0.16	76.24 ± 1.040

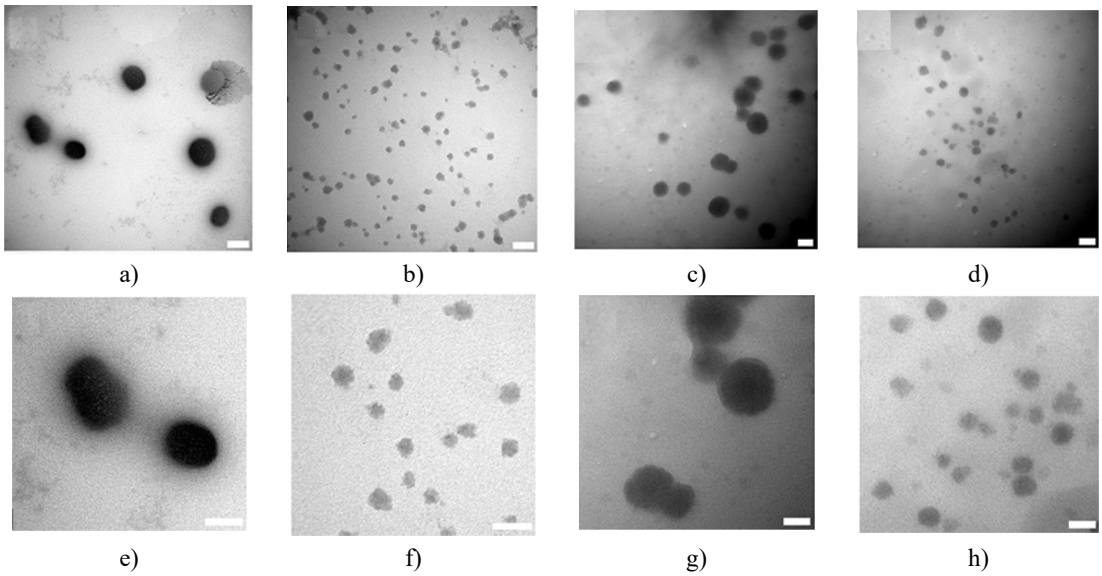

Figure 4. shows TEM images of the nanoparticles. Panels a and e represent PEI-DSH NPs, b and f show PEI-DSP NPs, c and g depict SA-PEI-DSH NPs, and d and h display SA-PEI-DSP NPs. The scale bars for a and b are 100 nm, for c and d are 200 nm, for e and f are 50 nm, and for g and h are 100 nm.

The in vitro stability of SA-PEI-DSH and SA-PEI-DSP NPs was evaluated, and the results are shown in **Figures 5a and 5b**. When incubated in media simulating different segments of the gastrointestinal tract, the particle size of SA-PEI-DDs NPs exhibited a similar trend: the most pronounced increase occurred in artificial gastric juice, followed by a slower growth in artificial intestinal juice, and the smallest change was observed in artificial colonic fluid. This behavior suggests that under strongly acidic conditions (pH 1.2), the abundant protons interact electrostatically with the negatively charged SA on the nanoparticle surface. In addition, protons can penetrate the NPs and create electrostatic repulsion with PEI, disrupting the multiple noncovalent interactions—such as electrostatic and hydrogen bonding forces—between DDs, PEI, and SA. This structural disturbance leads to a substantial increase in particle size.

As the pH increases, the influence of protons diminishes, resulting in a slower growth of particle size. Under mildly alkaline conditions (pH 7.4), electrostatic repulsion between negatively charged hydroxyl ions and surface SA helps maintain the structural integrity of the nanoparticles. The low concentration of hydroxyl ions exerts minimal effect on the internal noncovalent interactions of SA-PEI-DDs NPs, producing only slight increases in particle size. Notably, SA-PEI-DSP NPs exhibited smaller particle size increases than SA-PEI-DSH NPs under acidic conditions, likely because DSP carries more negative charges, which strengthen its electrostatic interactions with PEI and enhance the structural stability of the nanoparticles in acidic environments.

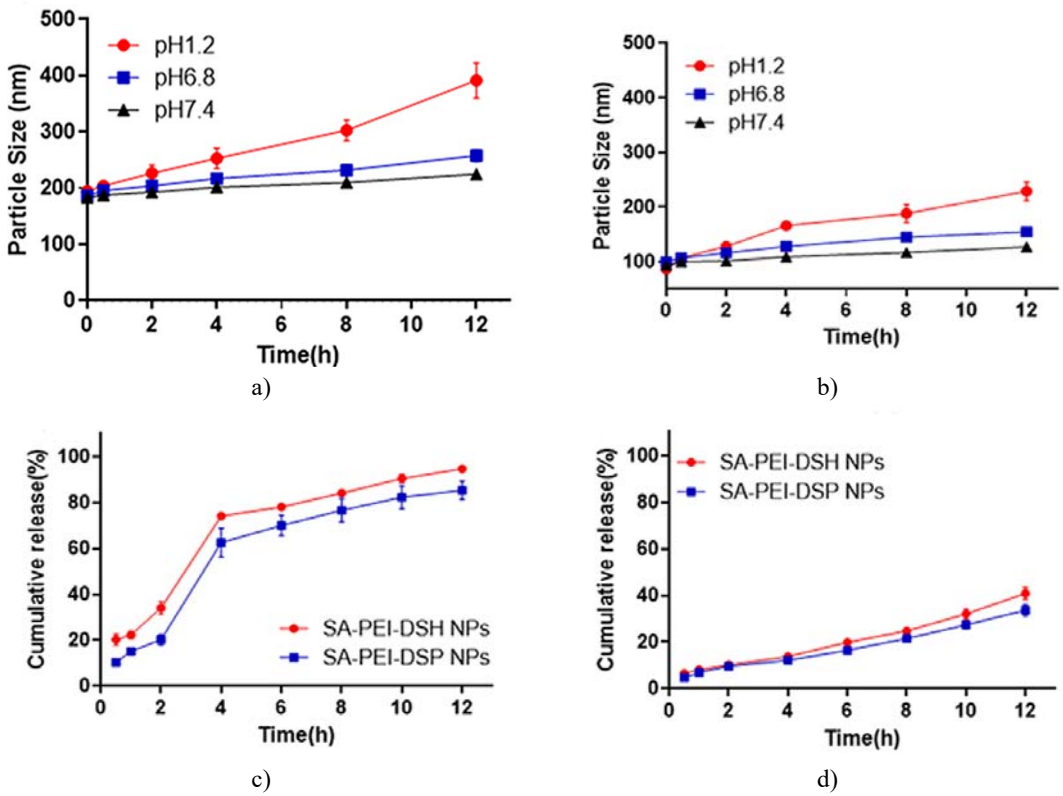

Figure 5. Illustrates the stability and in vitro release behavior of the nanoparticles. Panels A and B show the influence of media with different pH values on particle size changes for SA-PEI-DSH NPs (a) and SA-PEI-DSP NPs (b). Panels c and d depict the in vitro release profiles of SA-PEI-DDs NPs. For oral administration simulation **(Figure 5c)**, the experiment was conducted sequentially in media at pH 1.2 (0–2 h), pH 6.8 (3–6 h), and pH 7.4 (7–10 h). For enema administration simulation **(Figure 5d)**, the NPs were incubated in pH 7.4 medium for 12 h.

The release profiles demonstrated that under conditions mimicking oral administration, SA-PEI-DDs NPs exhibited a burst release in acidic environments, leading to rapid liberation of DDs. Notably, SA-PEI-DSP NPs released DDs more slowly than SA-PEI-DSH NPs at all time points, likely due to stronger electrostatic interactions between DSP and PEI, which stabilized the nanoparticles and slowed degradation. In contrast, under conditions simulating enema administration, both types of NPs showed a gradual release, reaching a cumulative release of approximately 40% over 12 h. These findings indicate that solution pH markedly influences the structural integrity and release behavior of SA-PEI-DDs NPs. Acidic conditions accelerate drug release by disrupting NP interactions, whereas alkaline conditions maintain NP stability, highlighting the suitability of these NPs for enema delivery, where they remain stable in colonic fluid and minimize premature drug leakage.

The mucoadhesive properties of SA-PEI-DDs NPs were evaluated through ex vivo and in vivo experiments. Ex vivo adhesion to isolated colonic mucosa was assessed by measuring reductions in the Kilo-count per second (Kcps) of light scattering, reflecting nanoparticle adsorption to the tissue [39, 40]. As shown in **Figure 6a**, in healthy colonic tissue, PEI-DDs NPs induced a greater reduction in Kcps than SA-PEI-DDs NPs ($p < 0.05$), likely due to electrostatic interactions between the positively charged PEI-DDs NPs and the negatively charged normal mucosa, enhancing adhesion. Additionally, PEI-DSP NPs showed a more pronounced Kcps decrease compared with PEI-DSH NPs, possibly because their smaller particle size facilitated greater tissue attachment. Conversely, in inflamed colonic tissue **(Figure 6b)**, SA-PEI-DDs NPs demonstrated larger reductions in Kcps relative to PEI-DDs NPs ($p < 0.05$), consistent with electrostatic attraction between the negatively charged nanoparticles and the positively charged inflamed mucosa.

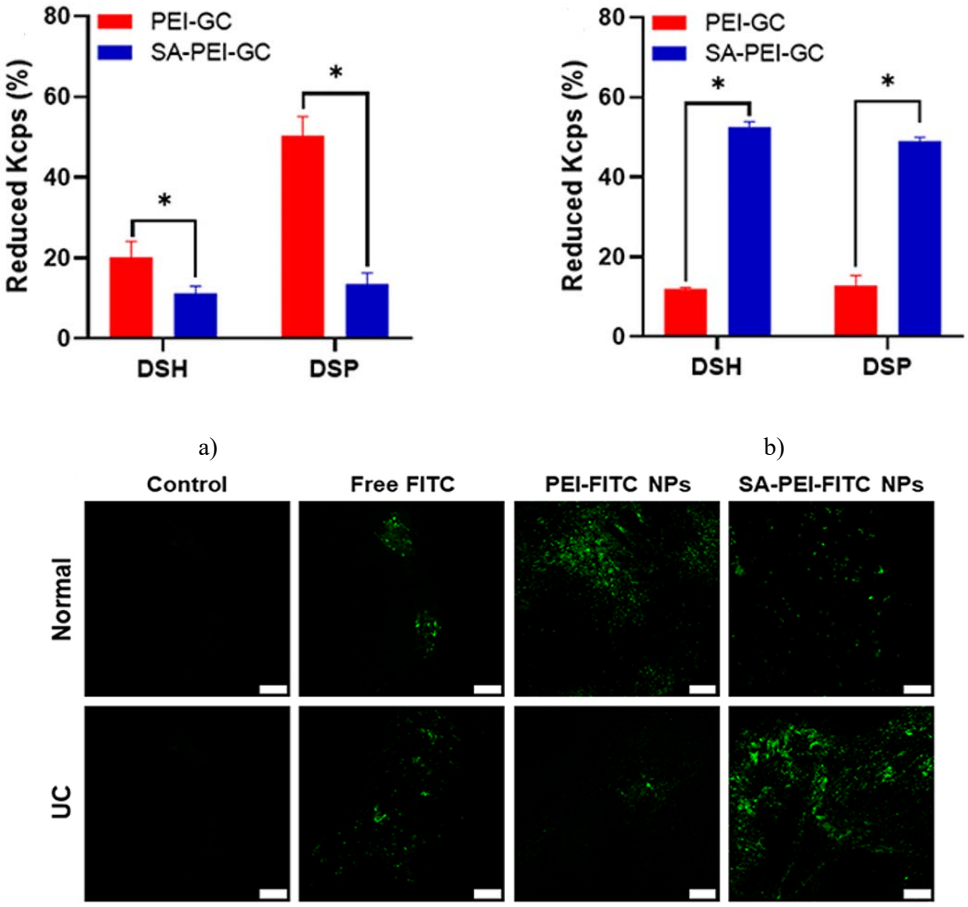

Figure 6. Illustrates both ex vivo and in vivo assessments of the mucoadhesive properties of SA-PEI-DDs NPs. Panels A and B show the adhesion of NPs to isolated colonic mucosa from healthy mice (a) and mice with ulcerative colitis (UC) (b). Significant differences compared with PEI-DDs NPs are indicated (*$p < 0.05$, mean ± SD, n = 3). Panel C presents confocal laser scanning microscopy (CLSM) images of colonic tissue following enema administration of different FITC formulations for 2 h (scale bars: 100 µm).

The in vivo adhesion of SA-PEI-DDs NPs was evaluated using FITC as a fluorescent surrogate for Dex due to its comparable molecular weight (Mn: 389 vs 392) and charge [41, 42]. SA-PEI-FITC NPs were administered via enema for 2 h, and the association of NPs with colonic tissue was visualized by CLSM. **Figure 6c** shows that both normal and UC mice receiving free FITC exhibited weak fluorescence. In normal mice, PEI-FITC NPs produced higher fluorescence than SA-PEI-FITC NPs. In contrast, UC mice treated with SA-PEI-FITC NPs demonstrated the strongest fluorescence among all groups. These findings indicate that negatively charged SA-PEI-FITC NPs preferentially adhered to positively charged inflamed mucosa, enhancing nanoparticle targeting to colonic lesions and increasing local drug concentration, consistent with the in vitro adhesion observations.

The therapeutic efficacy of the nanoparticles was further evaluated in an experimental colitis model over a 5-day period, during which all mice survived. Body weight loss is a key indicator of UC severity. **Figures 7a** show that, compared with the saline-treated control group, mice subjected to TNBS exhibited varying degrees of weight loss. Treatment with the nanoparticle formulations reversed this trend within 2 days, demonstrating their ability to mitigate TNBS-induced colitis. Notably, mice treated with SA-PEI-DDs NPs showed a greater recovery in body weight than those receiving free Dex, indicating superior therapeutic effects of the nanoparticle formulations.

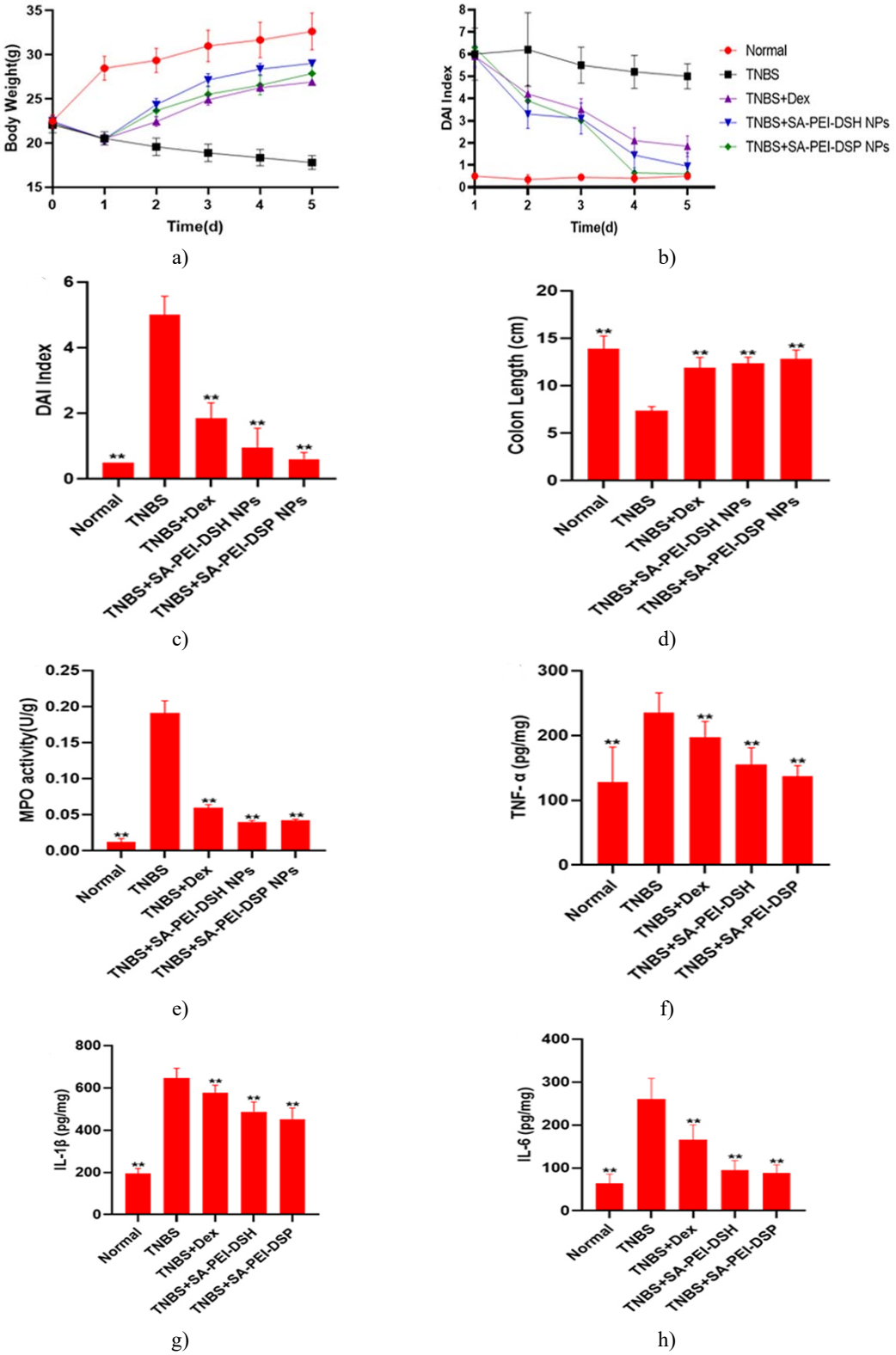

Figure 7. Illustrates the therapeutic effects of SA-PEI-DDs NPs on ulcerative colitis (UC). Panel a shows the changes in body weight of mice, panels b and c present the variations and final values of the disease activity index (DAI) after 5 days, panel d shows colon lengths, panel e depicts myeloperoxidase (MPO) activity, and panels F–H show the expression levels of TNF-α, IL-1β, and IL-6 in colonic tissues. Statistical significance compared with the TNBS-treated group is indicated (**$p < 0.01$, mean ± SD, n = 10).

Following TNBS-induced colitis, mice exhibited typical symptoms such as bloody stools, diarrhea, reduced activity, and weight loss within 24 hours. The DAI is a composite measure based on these parameters [35, 43, 44]. After TNBS modeling, both the TNBS-only group and all treatment groups displayed elevated DAI scores due to these symptoms. By the second day of treatment, DAI scores in all treatment groups except the TNBS-only group began to decrease. After 5 days, DAI values in the SA-PEI-DDs NPs groups were significantly lower than in the TNBS group ($p < 0.01$) and were also lower than those of the free Dex group. Remarkably, the final DAI scores of the SA-PEI-DDs NPs groups approached those of the normal group, indicating superior anti-inflammatory effects compared with free glucocorticoids **(Figures 7b and 7d).**

At the end of the experiment, mice were sacrificed and their colons collected for measurement **(Figure 7d)**. The TNBS group showed significant colon shortening compared with the normal group and treatment groups. Colon lengths in the NPs-treated groups were longer than in the free Dex group, suggesting improved protection against colonic injury.

MPO, a heme-containing enzyme found in neutrophils and monocytes, serves as a marker of myeloid cell infiltration and is widely used to assess inflammation severity, as its activity increases sharply under inflammatory conditions [45–47]. **Figure 7e** shows that MPO activity in the TNBS group was markedly elevated compared with the normal and treated groups ($p < 0.01$). Treatment with Dex or NPs significantly reduced MPO activity, with the NPs groups showing a greater reduction than free Dex, highlighting the superior anti-inflammatory efficacy of the nanoparticles.

Inflammatory cytokine levels also correlate with UC severity. As shown in **Figures 7f–7h**, TNF-α, IL-1β, and IL-6 concentrations in colon tissue were significantly reduced in all treatment groups compared with the TNBS group. Both NPs groups exhibited lower cytokine levels than the free Dex group, demonstrating enhanced mitigation of inflammatory responses. Notably, SA-PEI-DSP NPs consistently showed slightly better outcomes than SA-PEI-DSH NPs, likely due to stronger binding of DSP's additional negative charges to PEI, which improves delivery to the inflamed site. Additionally, the smaller particle size of SA-PEI-DSP NPs may enhance adhesion to the inflamed mucosa, facilitating targeted delivery through the enhanced epithelial permeability and retention (eEPR) effect.

Histopathological evaluation of the colon via H&E staining further confirmed the therapeutic effects **(Figure 8).** In normal mice, the colonic mucosal barrier was intact, glands were orderly, and lamina propria showed no inflammatory infiltration. Conversely, TNBS-induced mice exhibited disrupted mucosal barriers, edematous submucosa, abnormal gland structure, loss of crypts, and heavy inflammatory cell infiltration. In all treatment groups, the mucosal epithelium remained largely intact with reduced inflammation, and the histological appearance of colons treated with SA-PEI-DDs NPs closely resembled normal tissue, demonstrating substantial amelioration of colonic inflammation.

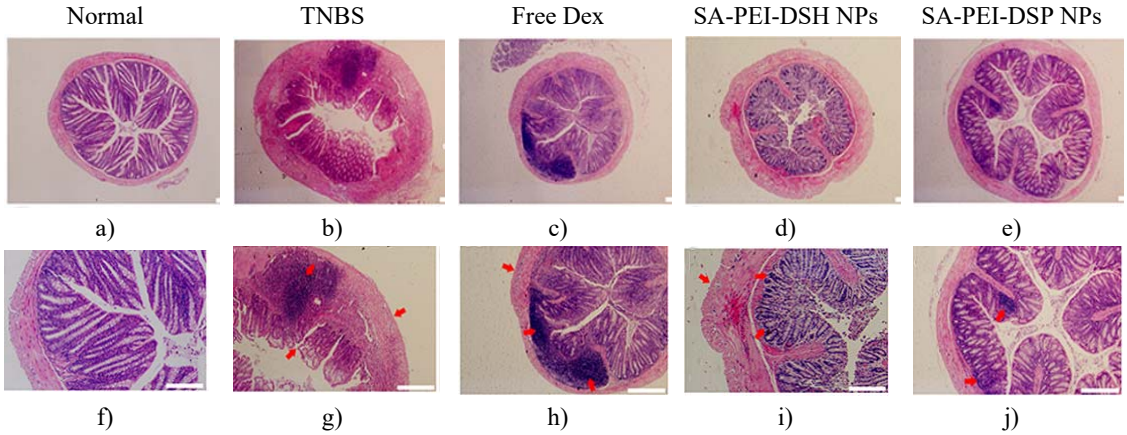

Figure 8. presents the histological evaluation of colonic sections stained with hematoxylin and eosin (H&E). Panels a–e show complete colon sections across different treatment groups, with scale bars of 200 μm, while panels f–j provide corresponding magnified views at 100 μm. In the TNBS group, the colon exhibited collapsed crypt structures, substantial inflammatory cell infiltration, and thickening of the intestinal wall. The free Dex-treated group still showed notable inflammatory infiltration and wall thickening. In the SA-PEI-DSH NPs group, partial colon regions displayed inflammation, with slight thickening of the intestinal wall.

For the SA-PEI-DSP NPs group, only localized inflammatory cell infiltration was observed in the colon tissue, indicating more effective protection compared with other treatments.

Conclusion

A novel mucoadhesive nanoparticle system was successfully developed. The core PEI-DDs nanoparticles were formed through electrostatic interaction between the negatively charged Dex derivatives and the positively charged PEI. Subsequently, an outer layer of negatively charged SA was coated via electrostatic adsorption to form the final SA-PEI-DDs nanoparticles. The final morphology of these nanoparticles was significantly influenced by variations in polymer concentration and pH during fabrication. The SA-PEI-DDs NPs demonstrated excellent stability and strong adhesion to inflamed colonic mucosa, promoting Dex accumulation at colitis sites and enhancing its therapeutic efficacy. In vivo studies of TNBS-induced experimental colitis confirmed that SA-PEI-DDs NPs provided superior anti-inflammatory effects compared with free Dex following enema administration. These findings indicate that mucoadhesive nanoparticles offer efficient colon-targeted delivery and hold considerable potential as a novel nano-enema therapy for ulcerative colitis.

Acknowledgments: The authors thank the Instrument Analysis Center of Xi'an Jiaotong University for the help and funding (Subsidy fund for the operation of large instruments and equipment, No. YB2022051) on the characterization.

Conflict of Interest: None

Financial Support: This work was supported financially by the National Natural Science Foundation of China (No. 81973253, 81803491, 81773663), the China Postdoctoral Science Foundation (No. 2021M702633), the Key R&D Program Project for Shaanxi Province (No. 2022SF-081, 2020SF-218), the Fundamental Research Funds for the Central Universities (No. xxj032021004) and the National Undergraduate Innovation and Entrepreneurship Training Program (No. S202110698182).

Ethics Statement: None

References

1. Ungaro R, Mehandru S, Allen PB, Peyrin-Biroulet L, Colombel JF. Ulcerative colitis. Lancet. 2017;389(10080):1756–70. doi:10.1016/S0140-6736(16)32126-2
2. Gajendran M, Loganathan P, Jimenez G, Catinella AP, Ng N, et al. A comprehensive review and update on ulcerative colitis. Dis Mon. 2019;65(12):100851. doi:10.1016/j.disamonth.2019.02.004. Epub 2019 Mar 2. PMID: 30837080.
3. Lorén V, Cabré E, Ojanguren I, Domènech E, Pedrosa E, García-Jaraquemada A, et al. Interleukin-10 enhances the intestinal epithelial barrier in the presence of corticosteroids through p38 MAPK activity in Caco-2 monolayers: a possible mechanism for steroid responsiveness in ulcerative colitis. PLoS One. 2015;10(6):e0130921. doi:10.1371/journal.pone.0130921. PMID: 26090671; PMCID: PMC4474693.
4. George LA, Cross RK. Treatment of ulcerative colitis with steroids (in whom, how long, what dose, what form). Gastroenterol Clin North Am. 2020;49(4):705–16. doi:10.1016/j.gtc.2020.08.001
5. Salice M, Rizzello F, Calabrese C, Calandrini L, Gionchetti P. A current overview of corticosteroid use in active ulcerative colitis. Expert Rev Gastroenterol Hepatol. 2019;13(6):557–61. doi:10.1080/17474124.2019.1604219
6. Van Molle W, Libert C. How glucocorticoids control their own strength and the balance between pro- and anti-inflammatory mediators. Eur J Immunol. 2005;35(12):3396–9. doi:10.1002/eji.200535556
7. Uchida K, Araki T, Toiyama Y, Yoshiyama S, Inoue M, Ikeuchi H, et al. Preoperative steroid-related complications in Japanese pediatric patients with ulcerative colitis. Dis Colon Rectum. 2006;49(1):74-9. doi:10.1007/s10350-005-0213-7. PMID: 16283565.
8. Oray M, Abu Samra K, Ebrahimiadib N, Meese H, Foster CS. Long-term side effects of glucocorticoids. Expert Opin Drug Saf. 2016;15(4):457–65. doi:10.1517/14740338.2016.1140743
9. Kayal M, Shah S. Ulcerative colitis: current and emerging treatment strategies. J Clin Med. 2020;9:1.

10. Cohen RD, Dalal SR. Systematic review: rectal therapies for the treatment of distal forms of ulcerative colitis. Inflamm Bowel Dis. 2015;21(7):1719–36. doi:10.1097/MIB.0000000000000379
11. Loew BJ, Siegel CA. Foam preparations for the treatment of ulcerative colitis. Curr Drug Deliv. 2012;9(4):338–44. doi:10.2174/156720112801323062
12. Hanauer S. Advantages in IBD: current developments in the treatment of inflammatory bowel diseases. Gastroenterol Hepatol (N Y). 2010;6(5):309–16.
13. Ham M, Moss AC. Mesalamine in the treatment and maintenance of remission of ulcerative colitis. Expert Rev Clin Pharmacol. 2012;5(2):113–23. doi:10.1586/ecp.12.2
14. Yan ZX, Liu YM, Ma T, Xu MJ, Zhang XB, Zha XJ, et al. Efficacy and safety of retention enema with traditional Chinese medicine for ulcerative colitis: a meta-analysis of randomized controlled trials. Complement Ther Clin Pract. 2021;42:101278. doi:10.1016/j.ctcp.2020.101278. Epub 2020 Nov 25. PMID: 33276227.
15. Tsuda M, Ohnishi S, Mizushima T, Hosono H, Yamahara K, et al. Preventive effect of mesenchymal stem cell culture supernatant on luminal stricture after endoscopic submucosal dissection in the rectum of pigs. Endoscopy. 2018;50(10):1001-16. doi:10.1055/a-0584-7262. Epub 2018 Apr 24. PMID: 29689574.
16. Beuerlein KG, Bowers NL, Savas J, Strowd LC. Ulcerative lesions and diarrhea: answer. Am J Dermatopathol. 2022;44(5):387–8. doi:10.1097/DAD.0000000000002081
17. Binder HJ. Mechanisms of diarrhea in inflammatory bowel diseases. In: Fromm M, Schulzke JD, editors. Molecular structure and function of the tight junction: from basic mechanisms to clinical manifestations. Vol. 1165. John Wiley & Sons; 2009:285–93.
18. Salim SY, Soderholm JD. Importance of disrupted intestinal barrier in inflammatory bowel diseases. Inflamm Bowel Dis. 2011;17(1):362–81. doi:10.1002/ibd.21403
19. Zhou HY, Ikeuchi-Takahashi Y, Hattori Y, Onishi H. Nanogels of a succinylated glycol chitosan-succinyl prednisolone conjugate: release behavior, gastrointestinal distribution, and systemic absorption. Int J Mol Sci. 2020;21:7.
20. Xu S, Yang Q, Wang R, Tian C, Ji Y, Tan H, et al. Genetically engineered pH-responsive silk sericin nanospheres with efficient therapeutic effect on ulcerative colitis. Acta Biomater. 2022;144:81-95. doi:10.1016/j.actbio.2022.03.012. Epub 2022 Mar 12. PMID: 35288310.
21. Jalanka J, Cheng J, Hiippala K, Ritari J, Salojärvi J, Ruuska T, et al. Colonic mucosal microbiota and association of bacterial taxa with the expression of host antimicrobial peptides in pediatric ulcerative colitis. Int J Mol Sci. 2020;21(17):6044. doi:10.3390/ijms21176044. PMID: 32842596; PMCID: PMC7504357.
22. Lj F, Gn F, Yy D, Lv P, Hy L. Bactericidal/permeability increasing protein gene polymorphism and inflammatory bowel diseases: meta-analysis of five case-control studies. Int J Colorectal Dis. 2017;32(3):433–5. doi:10.1007/s00384-016-2740-1
23. Zhang S, Ermann J, Succi MD, Zhou A, Hamilton MJ, Cao B, et al. An inflammation-targeting hydrogel for local drug delivery in inflammatory bowel disease. Sci Transl Med. 2015;7(300):300ra128. doi:10.1126/scitranslmed.aaa5657. PMID: 26268315; PMCID: PMC4825054.
24. Furuta R, Ando T, Watanabe O, Maeda O, Ishiguro K, Ina K, et al. Rebamipide enema therapy as a treatment for patients with active distal ulcerative colitis. J Gastroenterol Hepatol. 2007;22(2):261-7. doi:10.1111/j.1440-1746.2006.04399.x. PMID: 17295881.
25. Uppalapati D, Sharma M, Aqrawe Z, Coutinho F, Rupenthal ID, Boyd BJ, et al. Micelle directed chemical polymerization of polypyrrole particles for the electrically triggered release of dexamethasone base and dexamethasone phosphate. Int J Pharm. 2018;543(1-2):38-45. doi:10.1016/j.ijpharm.2018.03.039. Epub 2018 Mar 23. PMID: 29581065.
26. Fahira AI, Amalia R, Barliana MI, Gatera VA, Abdulah R. Polyethyleneimine (PEI) as a polymer-based co-delivery system for breast cancer therapy. Breast Cancer Targets Ther. 2022;14:71–83. doi:10.2147/BCTT.S350403
27. Wang X, Niu DC, Hu C, Li P. Polyethyleneimine-based nanocarriers for gene delivery. Curr Pharm Des. 2015;21(42):6140–56. doi:10.2174/1381612821666151027152907
28. Wegmann F, Gartlan KH, Harandi AM, Brinckmann SA, Coccia M, Hillson WR, et al. Polyethyleneimine is a potent mucosal adjuvant for viral glycoprotein antigens. Nat Biotechnol. 2012;30(9):883-8. doi:10.1038/nbt.2344. PMID: 22922673; PMCID: PMC3496939.

29. Kochkodan OD, Kochkodan VM, Sharma VK. Removal of Cu(II) in water by polymer enhanced ultrafiltration: influence of polymer nature and pH. J Environ Sci Health a Tox. 2018;53(1):33–8.
30. Helander IM, Latva-Kala K, Lounatmaa K. Permeabilizing action of polyethyleneimine on salmonella typhimurium involves disruption of the outer membrane and interactions with lipopolysaccharide. Microbiol UK. 1998;144:385–90. doi:10.1099/00221287-144-2-385
31. Dong WF, Liu D, Zhang TT, You Q, Huang FJ, Wu J. Oral delivery of staphylococcal nuclease ameliorates DSS induced ulcerative colitis in mice via degrading intestinal neutrophil extracellular traps. Ecotoxicol Environ Saf. 2021;215:1. doi:10.1016/j.ecoenv.2021.112161
32. Oshi MA, Lee J, Kim J, Hasan N, Im E, Jung Y, et al. pH-Responsive alginate-based microparticles for colon-targeted delivery of pure cyclosporine a crystals to treat ulcerative colitis. Pharmaceutics. 2021;13(9):1412. doi:10.3390/pharmaceutics13091412. PMID: 34575488; PMCID: PMC8469027.
33. Sonmez S, Coyle C, Sifrim D, Woodland P. Duration of adhesion of swallowed alginates to distal oesophageal mucosa: implications for topical therapy of oesophageal diseases. Aliment Pharmacol Ther. 2020;52(3):442–8. doi:10.1111/apt.15884
34. Nam YS, Kwon IK, Lee Y, Lee KB. Quantitative monitoring of corticosteroids in cosmetic products manufactured in Korea using LC-MS/MS. Forensic Sci Int. 2012;220(1–3):E23–E8. doi:10.1016/j.forsciint.2011.12.011
35. Dong K, Zhang H, Yan Y, Sun J, Dong Y, Wang K, et al. Improvement of side-effects and treatment on the experimental colitis in mice of a resin microcapsule-loading hydrocortisone sodium succinate. Drug Dev Ind Pharm. 2017;43(3):448-57. doi:10.1080/03639045.2016.1258410. Epub 2016 Nov 21. PMID: 27819157.
36. Sun W, Mao SR, Mei D, Kissel T. Self-assembled polyelectrolyte nanocomplexes between chitosan derivatives and enoxaparin. Eur J Pharm Biopharm. 2008;69(2):417–25. doi:10.1016/j.ejpb.2008.01.016
37. Mao SR, Bakowsky U, Jintapattanakit A, Kissel T. Self-assembled polyelectrolyte nanocomplexes between chitosan derivatives and insulin. J Pharm Sci. 2006;95(5):1035–48. doi:10.1002/jps.20520
38. Germershaus O, Mao SR, Sitterberg J, Bakowsky U, Kissel T. Gene delivery using chitosan, trimethyl chitosan or polyethylenglycol-graft-trimethyl chitosan block copolymers: establishment of structure-activity relationships in vitro. J Control Release. 2008;125(2):145–54. doi:10.1016/j.jconrel.2007.10.013
39. Yan Y, Sun Y, Wang P, Zhang R, Huo C, Gao T, et al. Mucoadhesive nanoparticles-based oral drug delivery systems enhance ameliorative effects of low molecular weight heparin on experimental colitis. Carbohydr Polym. 2020;246:116660. doi:10.1016/j.carbpol.2020.116660. Epub 2020 Jun 17. PMID: 32747292.
40. Sun W, Mao S, Wang Y, Junyaprasert VB, Zhang T, Na L, et al. Bioadhesion and oral absorption of enoxaparin nanocomplexes. Int J Pharm. 2010;386(1-2):275-81. doi:10.1016/j.ijpharm.2009.11.025. Epub 2009 Dec 1. PMID: 19958824.
41. Duff AF, Bielke LR, Relling AE. Technical note: fluorescein as an indicator of enteric mucosal barrier function in preruminant lambs. J Anim Sci. 2020;98:7. doi:10.1093/jas/skaa198
42. Joshi A, Keerthiprasad R, Jayant RD, Srivastava R. Nano-in-micro alginate based hybrid particles. Carbohydr Polym. 2010;81(4):790–8. doi:10.1016/j.carbpol.2010.03.050
43. Dong K, Zeng A, Wang M, Dong Y, Wang K, Guo C, et al. In vitro and in vivo study of a colon-targeting resin microcapsule loading a novel prodrug, 3, 4, 5-tributyryl shikimic acid. RSC Advances. 2016;6(20):16882-90.
44. Yan Y, Ren FL, Wang PC, Sun Y, Xing JF. Synthesis and evaluation of a prodrug of 5-aminosalicylic acid for the treatment of ulcerative colitis. Iran J Basic Med Sci. 2019;22(12):1452–61. doi:10.22038/IJBMS.2019.13991
45. Pinkus GS, Pinkus JL. Myeloperoxidase - a specific marker for myeloid cells in paraffin sections. Modern Pathol. 1991;4(6):733–41.
46. McCabe AJ, Dowhy M, Holm BA, Glick PL. Myeloperoxidase activity as a lung injury marker in the lamb model of congenital diaphragmatic hernia. J Pediatr Surg. 2001;36(2):334–6. doi:10.1053/jpsu.2001.20709
47. Tsai MS, Shaw HM, Li YJ, Lin MT, Lee WT, Chan KS. Myeloperoxidase in chronic kidney disease: role of visceral fat. Nephrology. 2014;19(3):136–42. doi:10.1111/nep.12187